Electronic Supplementary Material (ESI) for Nanoscale.

Unravelling the Atomistic Mechanisms Underpinning the Morphological Evolution of Al-alloyed Hematite

Jinxing Gu [a], Sasha Yang [a], Jefferson Zhe Liu [b]*, Lian Zhang [a]*

[a] Department of Chemical and Biological Engineering, Monash University, Victoria, 3800, Australia

[b] Department of Mechanical Engineering, Faculty of Engineering and Information Technology, The University of Melbourne, Victoria 3010, Australia

KEYWORDS: Aluminium-alloyed hematite; Morphology of nanoparticles; Density Functional Theory calculations; Cluster expansion; Monte Carlo simulations

Details for Cluster Expansion Method

The cluster expansion extends the well-known Ising model to map alloy configuration with the formation energy of (Fe, Al)$_2$O$_3$ alloy.[1] In the cluster expansion formulation, a spinor (s_i, i is the lattice site index) is assigned to each iron/aluminium occupation lattice site. Different values of s_i represent different atomic species, *e.g.*, $s_i = -1$ for the i^{th} site occupied by Fe and $s_i = +1$ for the i^{th} site occupied by Al. A crystal structure with a specific site occupancy order is called a configuration (σ), mathematically expressed as a vector $\boldsymbol{\sigma} = (s_1, s_2, s_3, \ldots s_N)$. A (Fe, Al)$_2O_3$ alloy breaks down into clusters such as zero-let, singlets, pairs, triplets, and quadruplets. Each cluster contains a group of lattice sites $\alpha = (p_1, p_2, \ldots, p_{n_\alpha})$. For a binary alloy, a multisite cluster function $\Phi_\alpha(\sigma)$ is defined as

$$\Phi_\alpha(\sigma) = s_{p_1} s_{p_1} \ldots s_{p_{n_\alpha}} . \#(1)$$

The symmetry-equivalent clusters can be grouped as an orbit, Ω_α. The orbit has an average multisite cluster function ($\hat{\Phi}_\alpha(\sigma)$):

$$\hat{\Phi}_\alpha(\sigma) = \frac{1}{N_\alpha} \sum_{\beta \in \Omega_\alpha} \Phi_\beta(\sigma), \#(2)$$

where N_α is the number of equivalent clusters in an orbit. The configuration-dependent physical quantity $F(\sigma)$ can be expressed as a weighted sum of multisite cluster functions:

$$F_{CE}(\sigma) = \sum_{\Omega_\alpha} J_\alpha N_\alpha \hat{\Phi}_\alpha(\sigma), \#(3)$$

where the effective-cluster interaction (ECI) coefficient J_α will be trained/fitted based on the DFT calculations for a set of configurations. Then, the per lattice site physical quantity is,

$$\frac{F_{CE}(\sigma)}{N} = \sum_{\Omega_\alpha} J_\alpha m_\alpha \hat{\Phi}_\alpha(\sigma), \#(4)$$

where $m_\alpha = N_a/N$ is the number of type α clusters per lattice site.[1] In this work, the configuration-dependent physical quantity $F(\sigma)$ is defined as the mixing energy per cation, per

$$\Delta E_{mix}(\sigma) = E_\sigma - (1-x)E_{Fe_2O_3} - xE_{Al_2O_3}, \#(5)$$

Where E_σ is the total energy per cation of configuration σ. The ECI coefficient J_α was determined by fitting $F_{\mathrm{CE}}(\sigma)$ (Eq. 4) to the DFT calculation results of $\Delta E_{\mathrm{mix}}(\sigma)$ for a set of configurations. The cut-off radius for pairs, triplets, and quadruplets was optimised to be 8.0, 4.5, and 4.5 Å, respectively. A good fit was obtained with 125 configurations using 97 pairs, 34 triplets, and 15 quadruplets through preliminary trial and error. The final cross-validation score value is set at 3.503 meV/atom. Hence, the CE model is converged.

Finally, the Metropolis Monte Carlo simulations under the canonical ensemble (NVT) were performed using the CE energy functional. The simulation cells contain 48,000 Fe/Al atoms. We examined multiple Al concentration cases from 1 at.% to 10 at.% and from 90 at.% to 99 at.% with a step size of 1 at.% and from 10 at.% to 90 at.% with a step size of 10 at.%. At a given Al concentration, MC simulations were performed at various temperatures from 100 to 1100 K. Accordingly, we can determine the phase transition temperature by inspecting the internal energy *vs*. temperature variation and heat capacity *vs*. temperature.

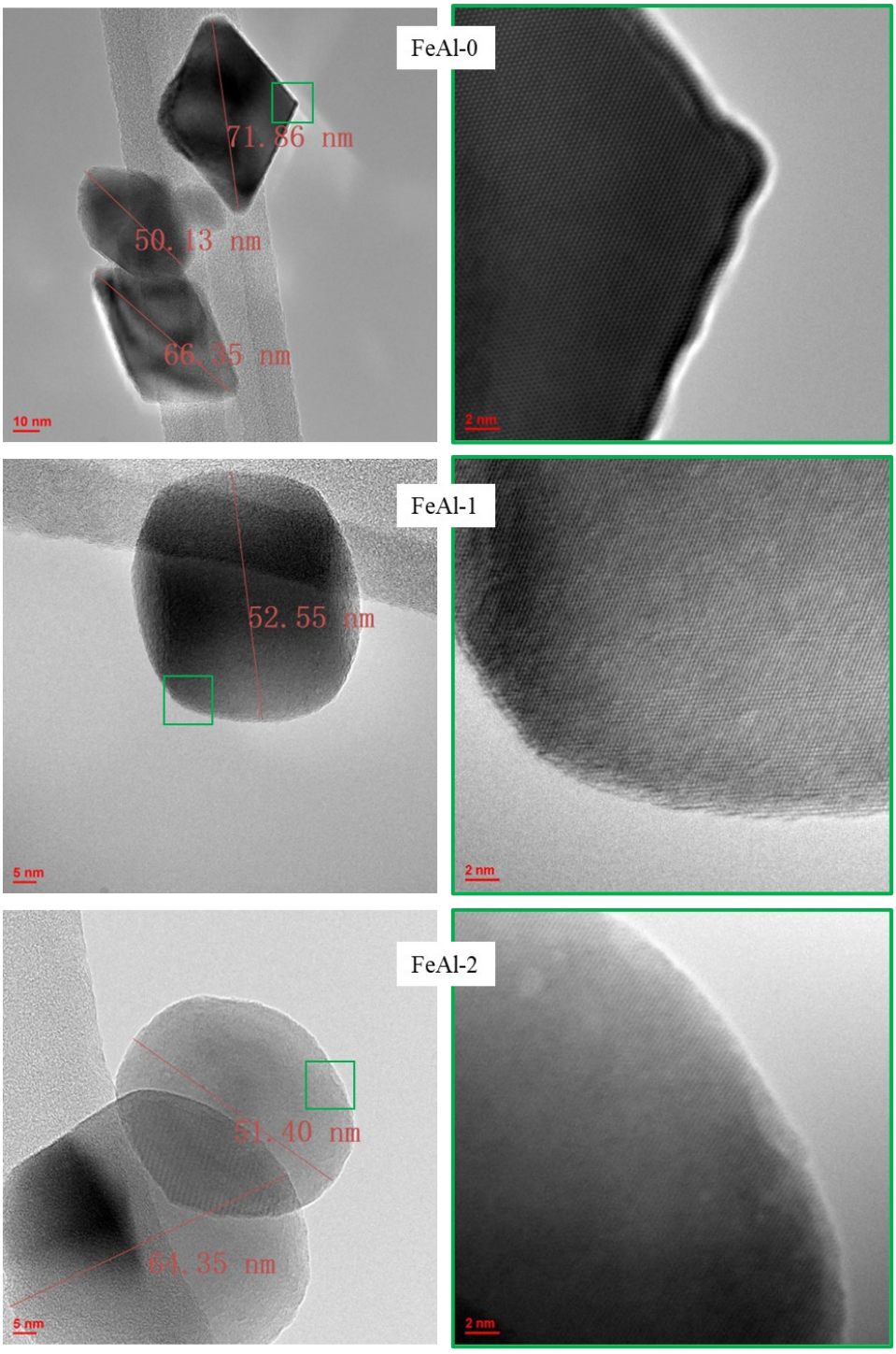

Figure S1. High-resolutionTEM image of FeAl-0, FeAl-1, and FeAl-2 nanoparticles showing their single crystal nature.

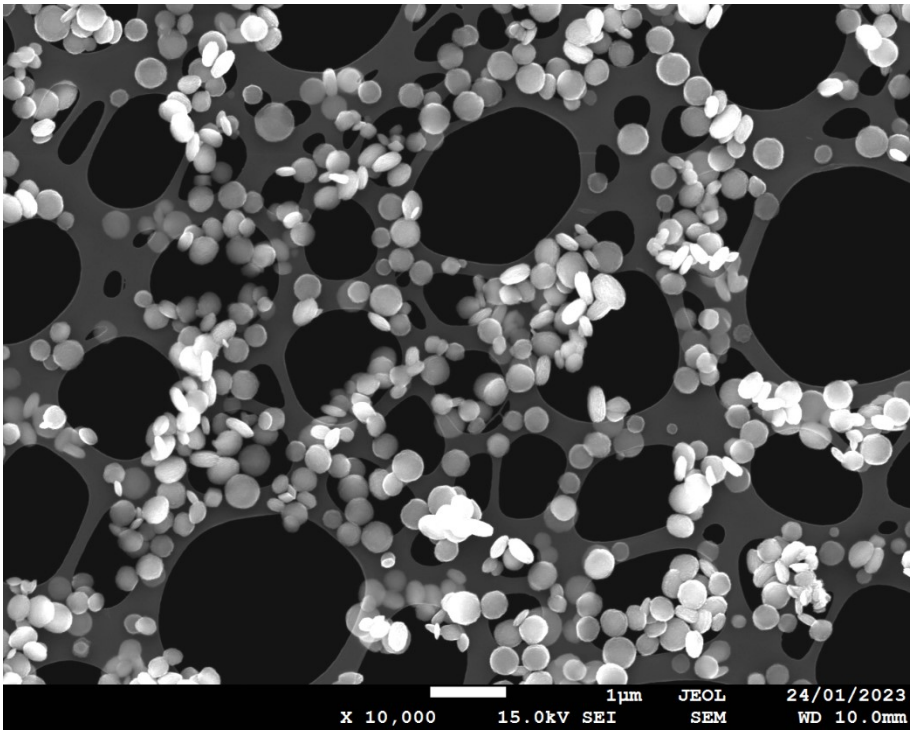

Figure S2. SEM image indicates the nanoparticle morphology of the FeAl-4 sample. Shapes other than round nanoplate belong to the side view of the round nanoplate.

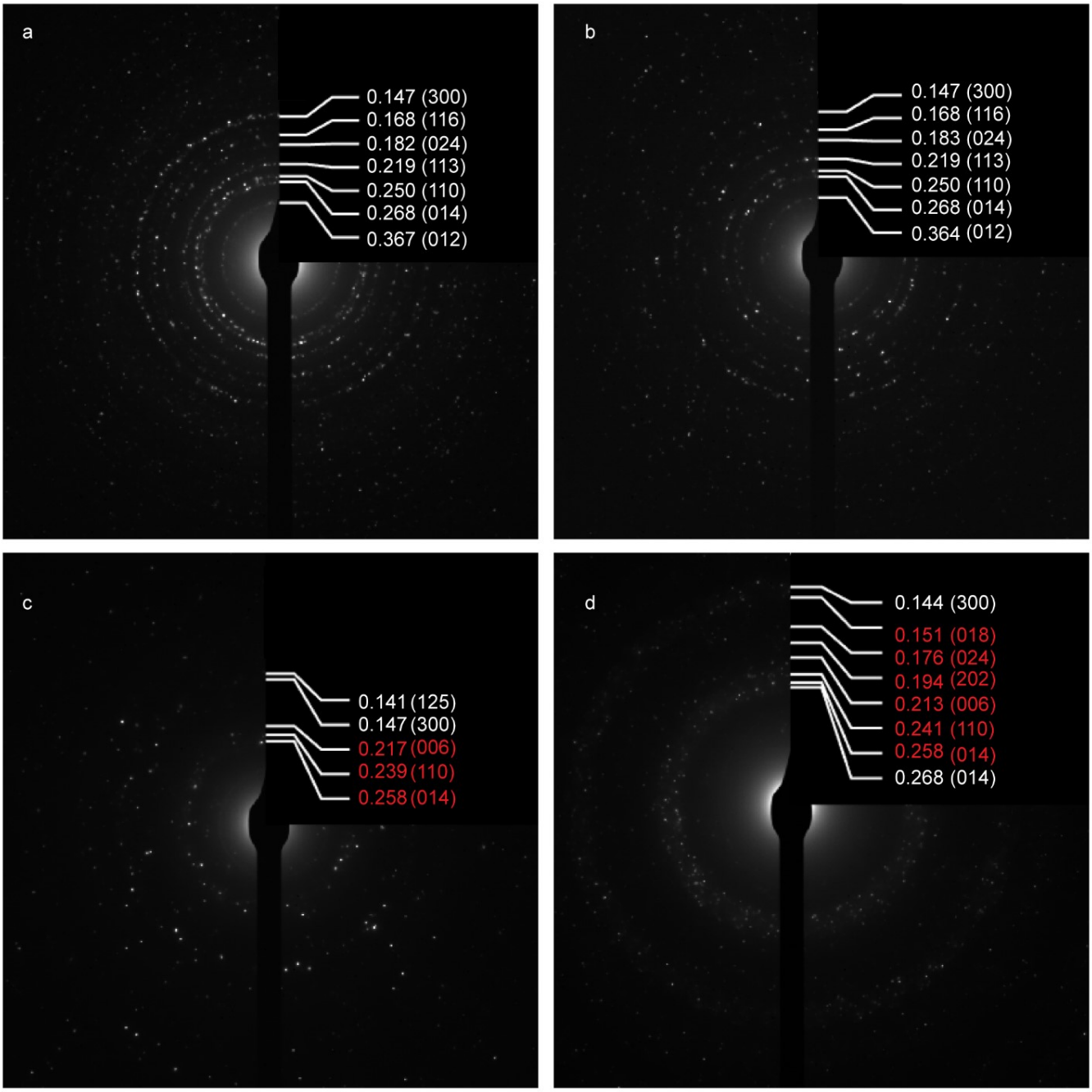

Figure S3. Ring diffraction pattern of (a) FeAl-1, (b) FeAl-2, (c) FeAl-3, and (d) FeAl-4. In each figure, values of the left column are the measured d-spacing (nm), and values of the right column are the identified lattice planes, white for hematite and red for corundum. The identifications were based on the following two tables, Table S1 and Table S2.

Table S1. d-spacings of lattice planes of corundum, taken from Ref.[2]

Plane	d-spacing (nm)	Plane	d-spacing (nm)
(012)	0.348	(006)	0.216
(014)	0.255	(113)	0.208
(110)	0.238	(202)	0.196
(024)	0.174	(018)	0.151

Table S2. d-spacings of lattice planes of hematite, taken from Ref.[3]

Plane	d-spacing (nm)	Plane	d-spacing (nm)
(012)	0.367	(116)	0.167
(014)	0.270	(113)	0.220
(110)	0.250	(300)	0.144
(024)	0.184	(018)	0.158

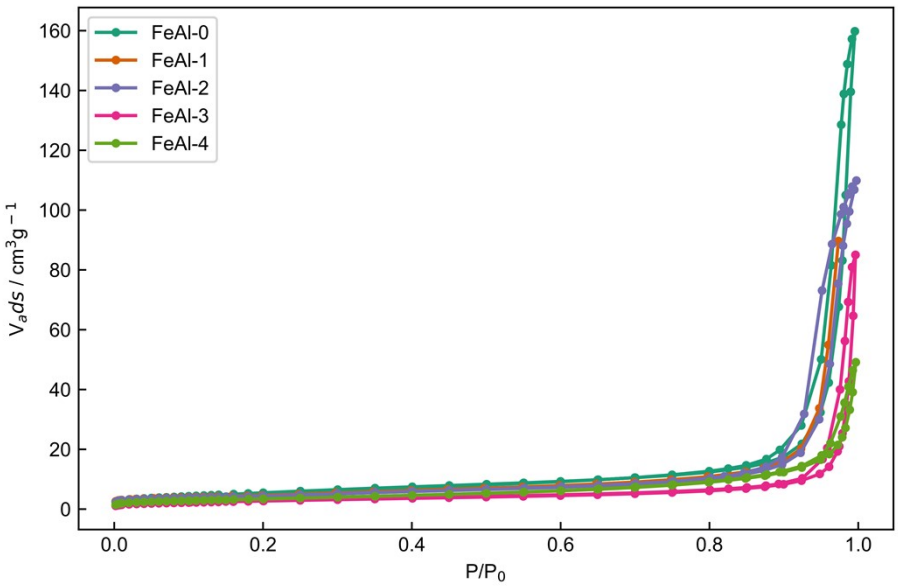

Figure S4. N_2 adsorption-desorption isotherm of FeAl-0, FeAl-1, FeAl-2, FeAl-3, and FeAl-4, showing the mesoporous characteristic.

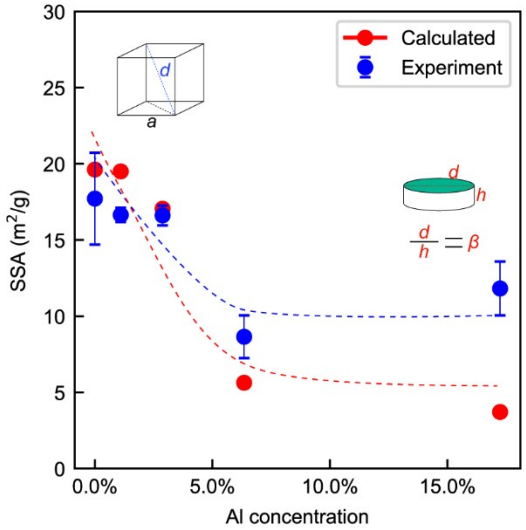

Figure S5. Experimental obtained and calculated SSA for the five samples.

Using a cube model, we also estimated the specific surface area of samples FeAl-0, FeAl-1, and FeAl-2. The SSA was calculated as

$$SSA = \frac{S}{m} = \frac{6a^2}{\rho a^3} = \frac{6}{\rho a} = \frac{6\sqrt{3}}{\rho d}$$

where S is the total surface area, m the mass, ρ the density of hematite, which is 7.874 g/cm^3, and a is the side length of the cube. In our estimations, d is the average size of the nanoparticle, and $d = \sqrt{3}a$. The SSA of samples FeAl-3 and FeAl-4 were estimated using a cylinder model. The SSA was calculated as

$$SSA = \frac{S}{m} = \frac{\frac{\pi d^2(0.5\beta + 1)}{\beta}}{\frac{0.25\pi\rho d^3}{\beta}} = \frac{2\beta + 4}{\rho d}$$

where β is the aspect ratio, and d is the diameter. In our estimations, d is also the average size of the nanoparticle.

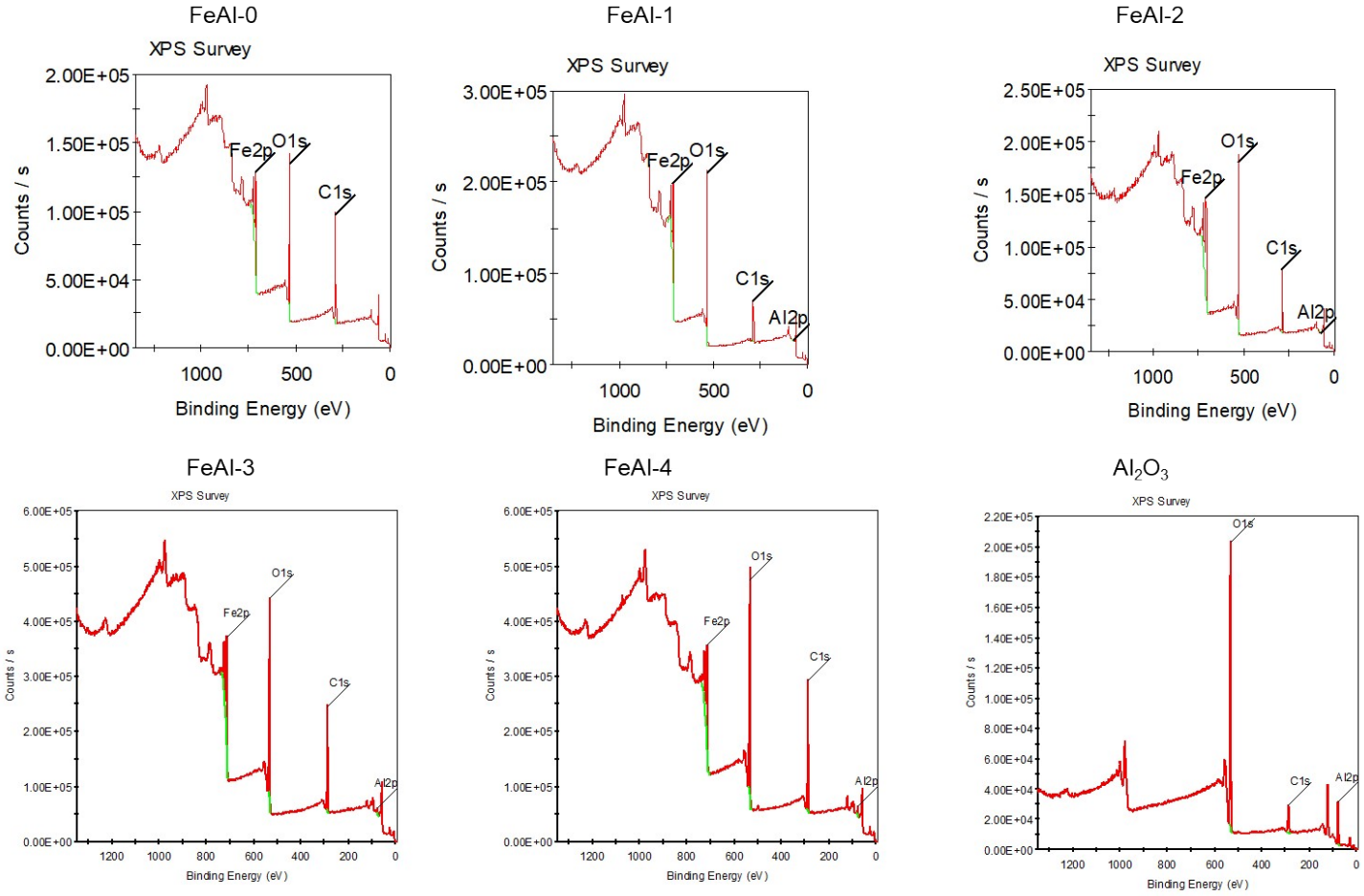

Figure S6. XPS examinations of five samples and a purchased α-Al_2O_3 reference.

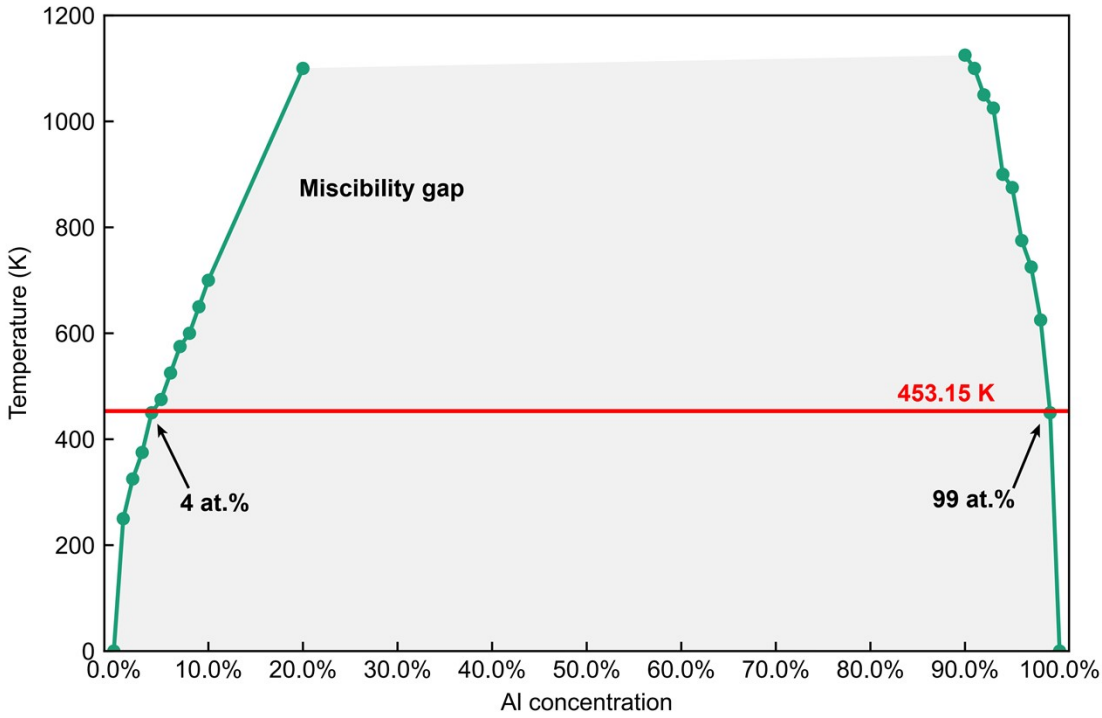

Figure S7. Phase diagram of $(Fe, Al)_2O_3$ alloy.

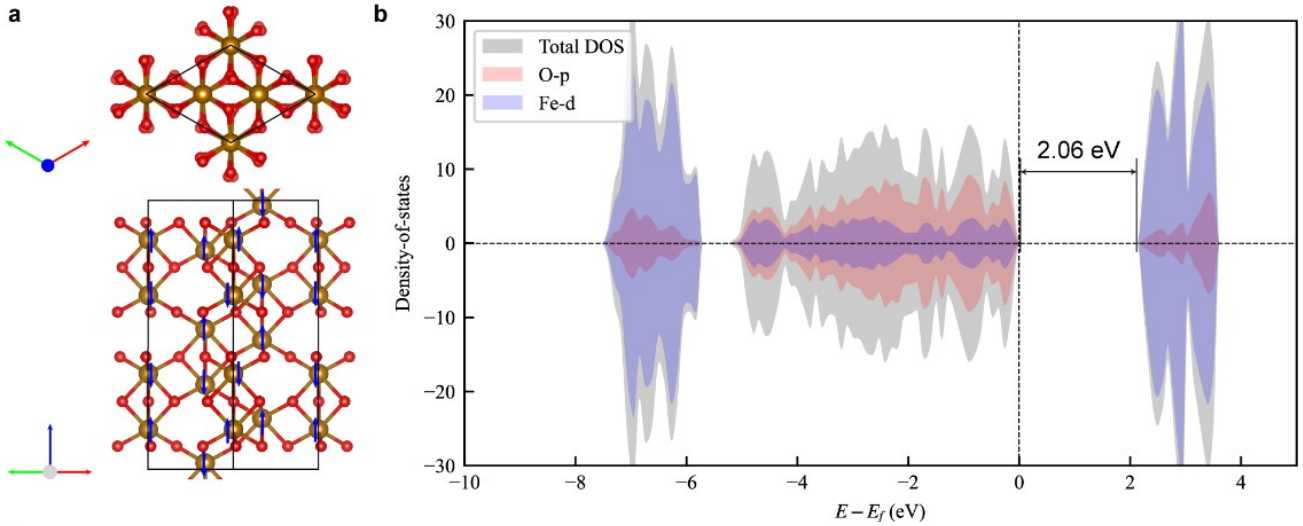

Figure S8. (a) The unit cell of α-Fe_2O_3 and (b) the computed density-of-states. The direction of the magnetic moment for each Fe is indicated by the blue arrows in (a).

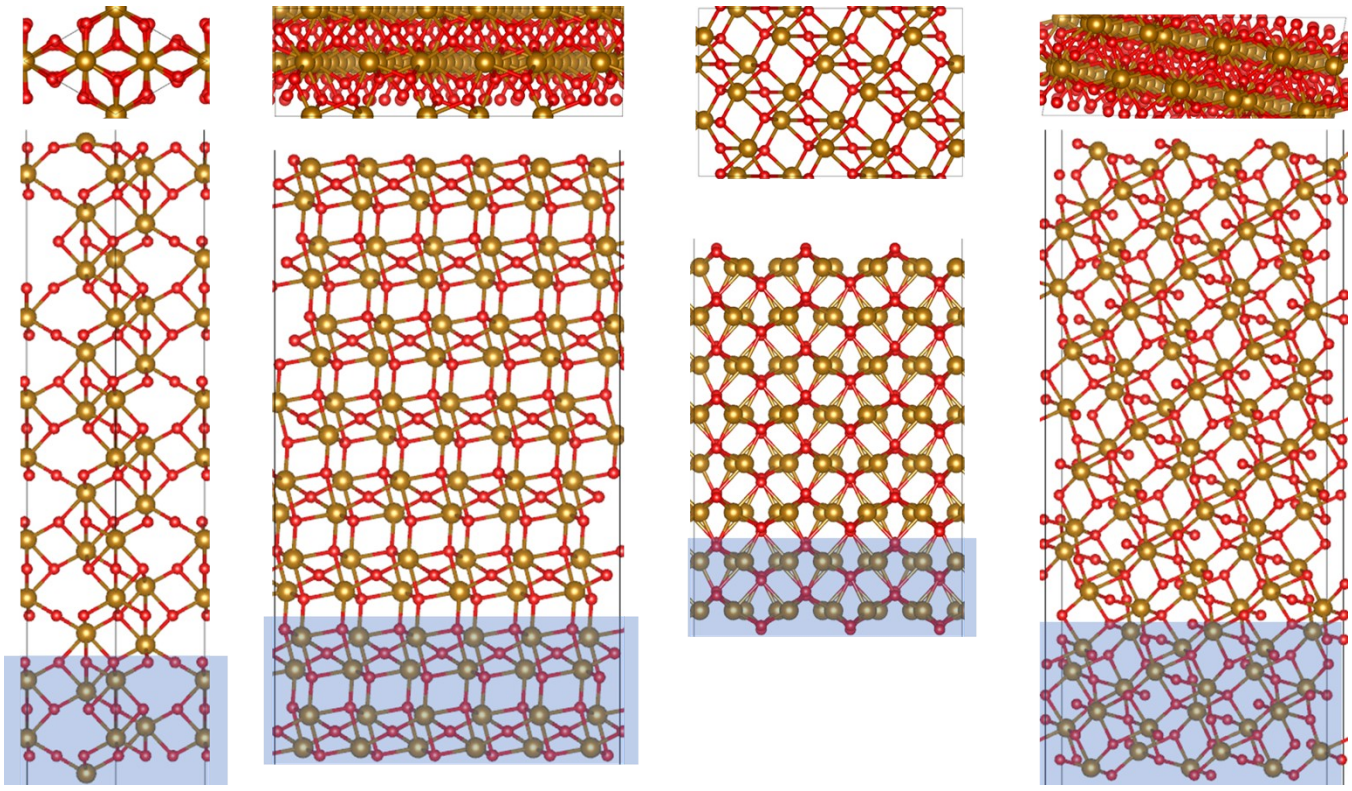

Figure S9. Top and side views of surface models used to compute the specific surface energy for (001), (012), (110), and (101) surfaces. The shaded areas indicate the atoms being fixed during the optimisation. The (001) surface model contains 70 atoms, while other models contain 240 atoms.

Specific surface energies validated by various methods

The specific surface energies (γ) were further validated using the other two methods. We labelled the method in the manuscript as Method I, and the other methods are Method II and Method III. Method II is expressed as,

$$\gamma = \frac{E_{surf}^{''} - NE_{bulk}}{2A}$$

where $E_{surf}^{''}$ is the energy of the surface model with both the top and the bottom sides being relaxed. E_{bulk} is the energy of bulk hematite per molecular formula unit. *N* is the number of molecular formulas of the surface model, and A is the area of the surface.

Method III is a linear fitting method, as demonstrated by Scholz and Stirner, to show the best convergence in calculating the specific surface energy of the hematite (001) surface.[4] The expression of Method III can be derived from Method II as,

$$E_{surf}^{''} = NE_{bulk} + 2A\gamma$$

This method finds that the energy of the surface model is linearly dependent on the value of *N*. The slope is the energy of the bulk per molecular formula unit, and the intercept is $2A\gamma$. The specific surface energies calculated by the three methods are listed in Table S1. All three methods yield identical or similar specific surface energy for each surface.

Table S3. Specific surface energies γ (in the unit of J/m^2) of pure hematite.

Surfaces	Method I	Method II	Method III	Ref.[5]	Ref.[6]	Ref.[7]	Ref.[8]
(001)	1.33	1.33	1.33	1.53	0.76	1.14	2.30
(012)	1.22	1.22	1.22	1.47	0.54	1.06	1.96
(110)	1.41	1.43	1.43	-	0.81	1.23	-
(101)	1.44	1.44	1.44	2.41	1.16	1.31	2.84

Coverage-dependent specific surface energy

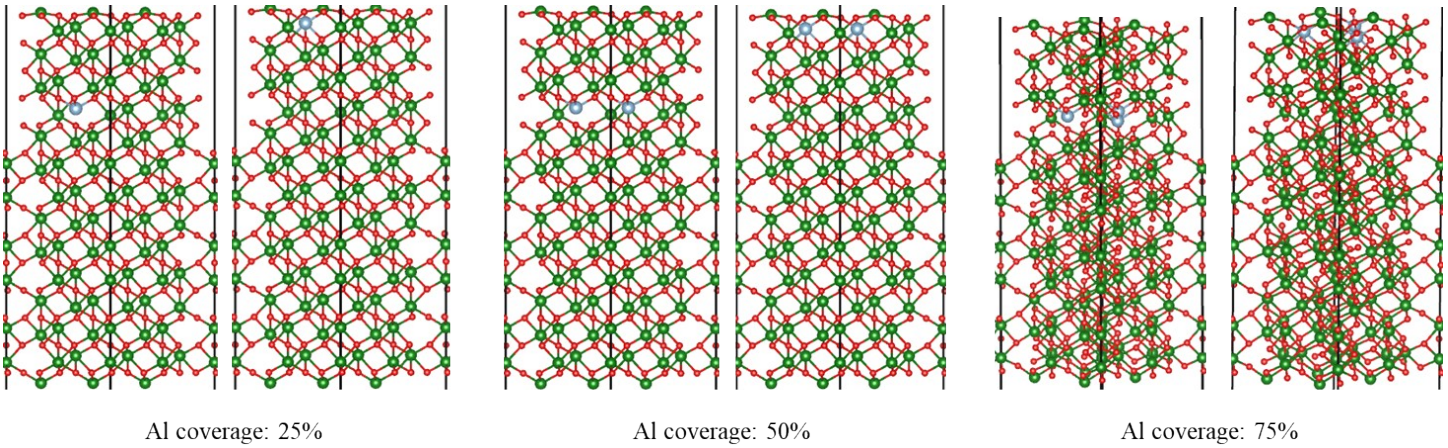

Figure S10. Model of (001) surface with various Al coverage for E_{seg} calculations. Green balls represent Fe atoms.

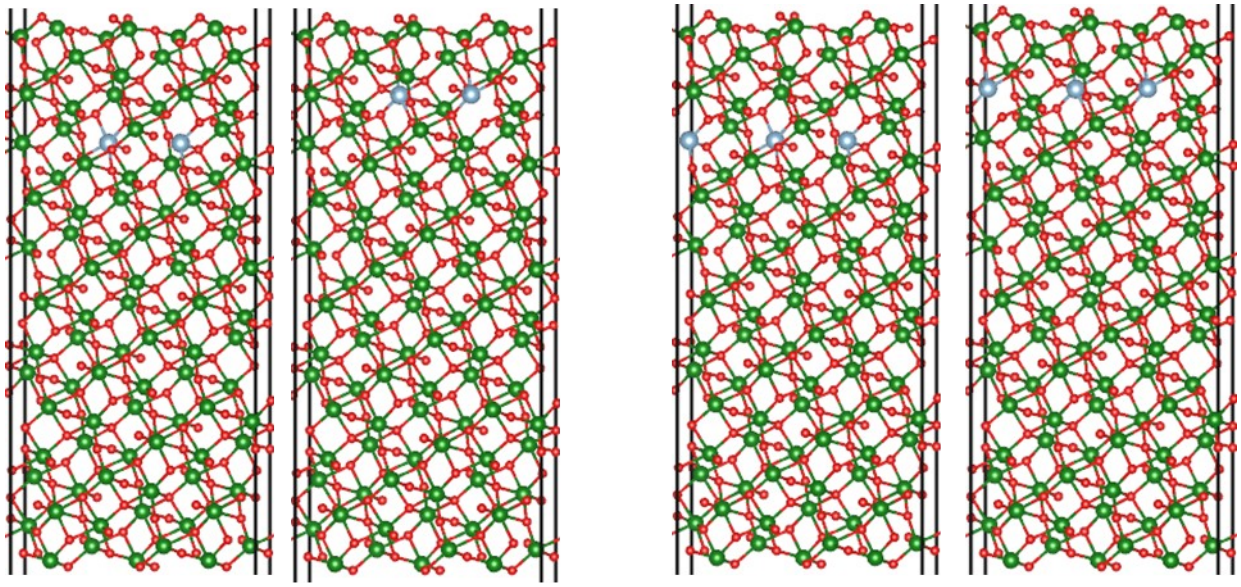

Figure S11. Models of surface (101) with various Al coverage for E_{seg} calculations. Green balls represent Fe atoms.

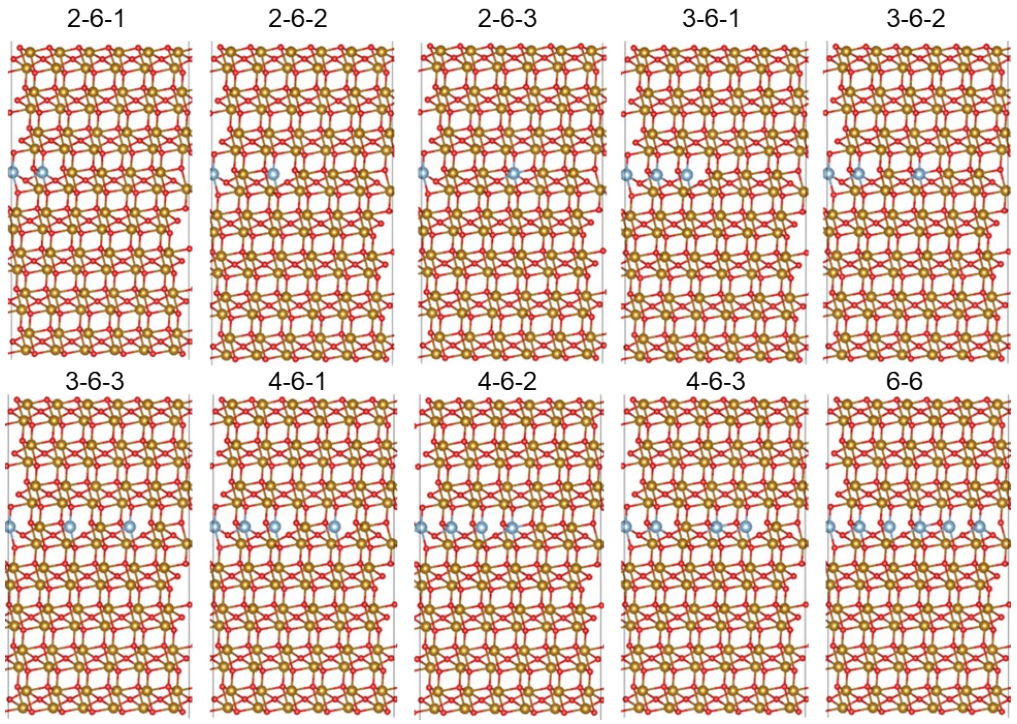

Figure S12-1. Models of surface (012) with 33.33%, 50%, 66.67%, and 100% Al coverage for finding the most stable configuration at the seventh layer. Orange balls represent Fe atoms.

Table S4. Relative energies of various configurations at some converge of surface (012).

Configurations	Energy	Configurations	Energy	Configurations	Energy
2-6-1	0.000	3-6-1	0.000	4-6-1	0.036
2-6-2	0.036	3-6-2	0.039	4-6-2	0.000
2-6-3	0.038	3-6-3	0.075	4-6-3	0.040

The relative energies show that energies of various configurations at the same coverage are close to each other.

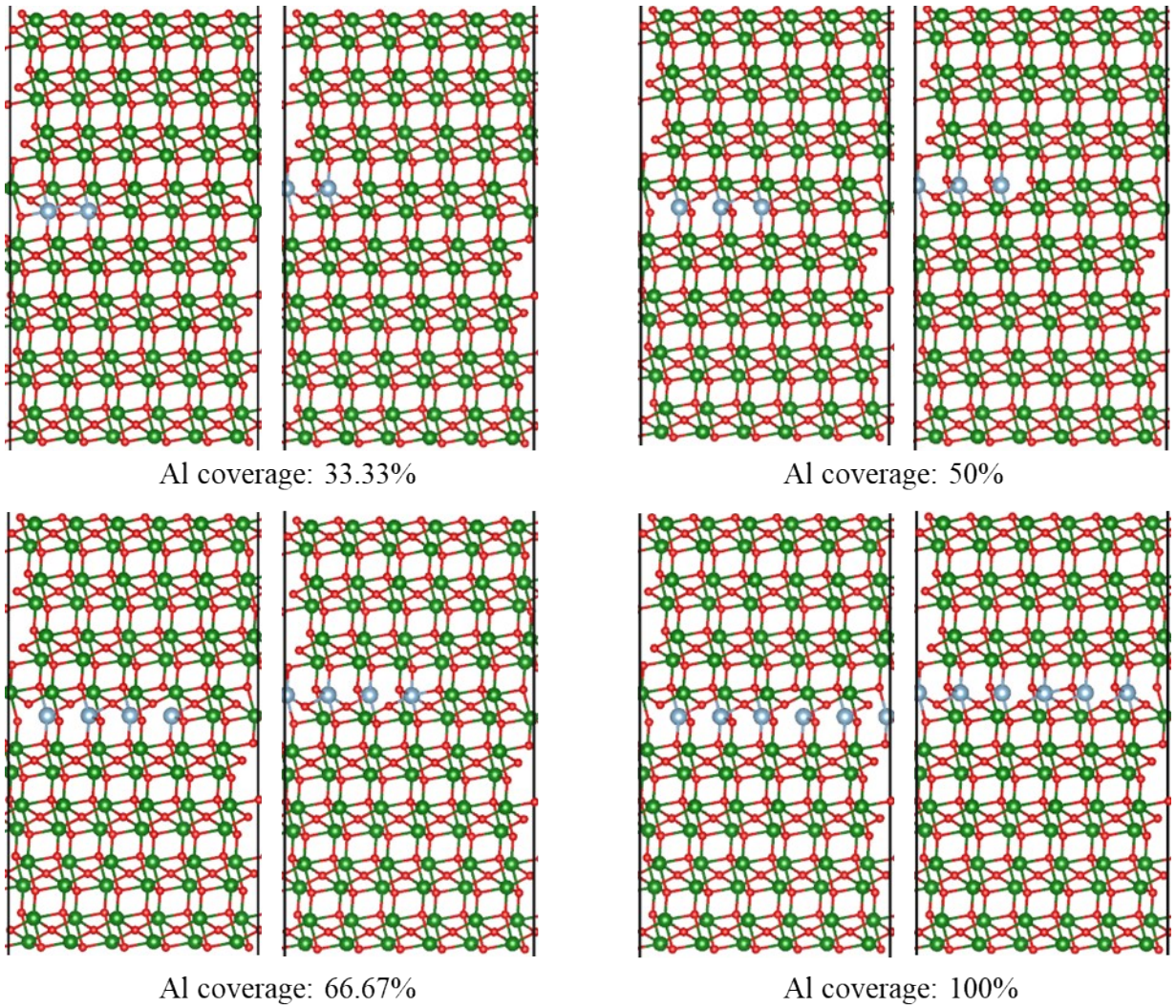

Figure S12-2. Model of (012) surface with various Al coverage for E_{seg} calculations. Green balls represent Fe atoms.

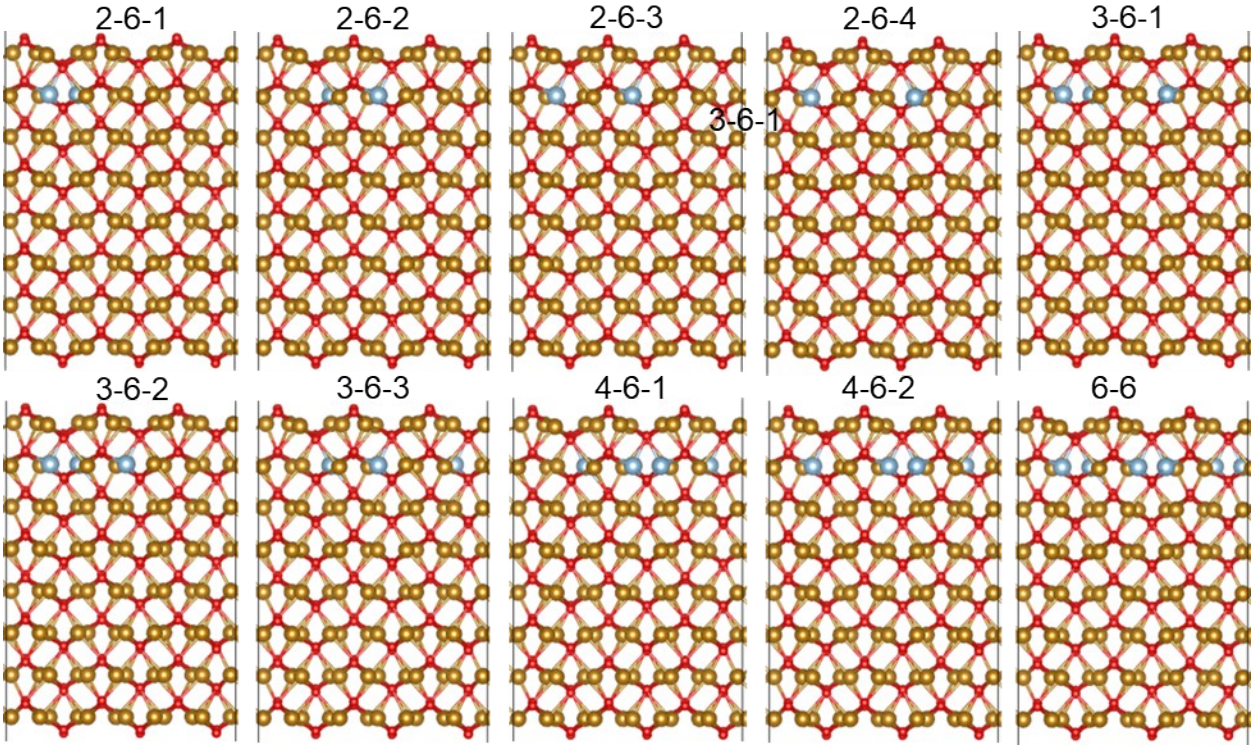

Figure S13-1. Models of surface (110) with 33.33%, 50%, 66.67%, and 100% Al coverage for finding the most stable configuration at the seventh layer. Orange balls represent Fe atoms.

Table S5. Relative energies of various configurations at some converge of surface (110).

Configurations	Energy	Configurations	Energy	Configurations	Energy
2-6-1	0.088	3-6-1	0.000	4-6-1	0.000
2-6-2	0.000	3-6-2	0.040	4-6-2	0.151
2-6-3	0.171	3-6-3	0.338		
2-6-4	0.023				

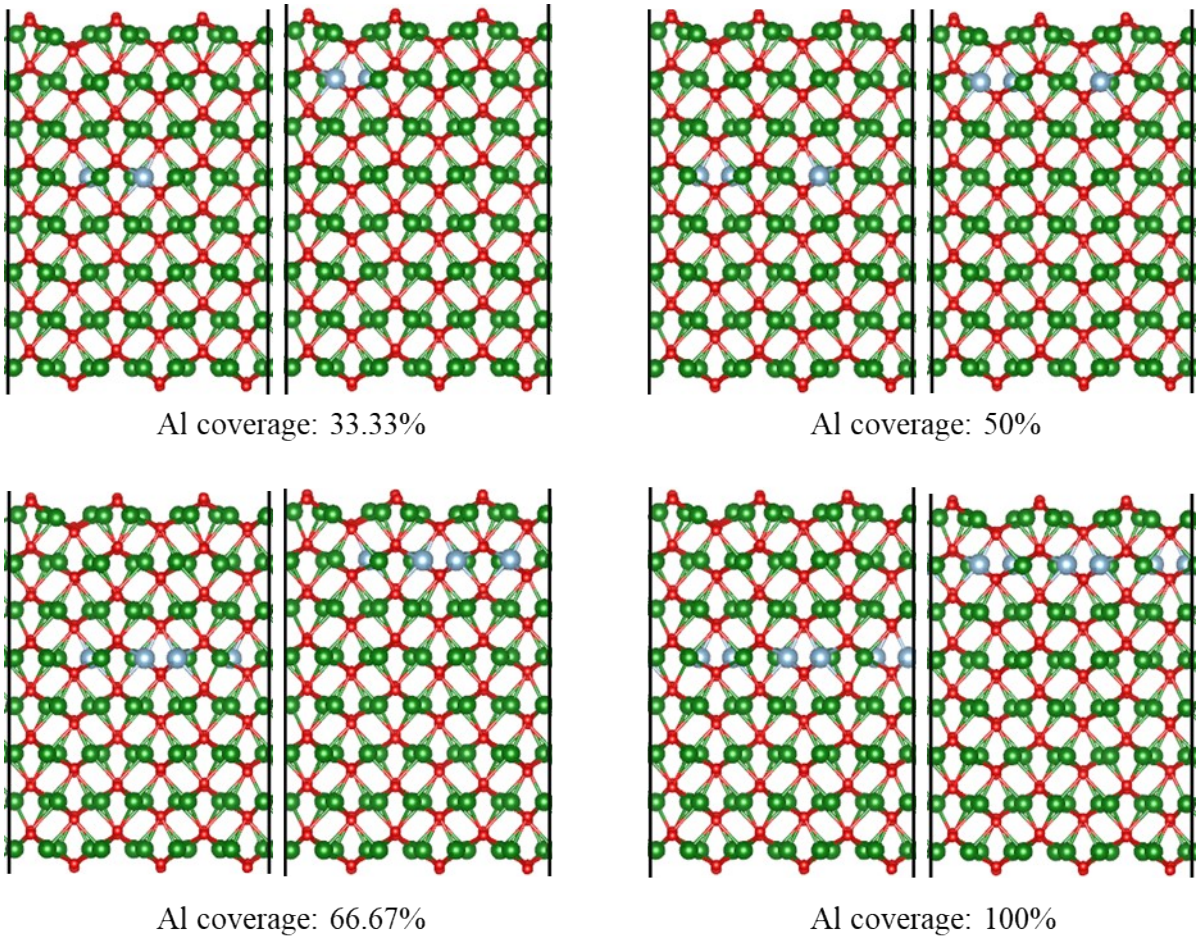

Figure 13-2. Model of (110) surface with various Al coverage for E_{seg} calculations. Green balls represent Fe atoms.

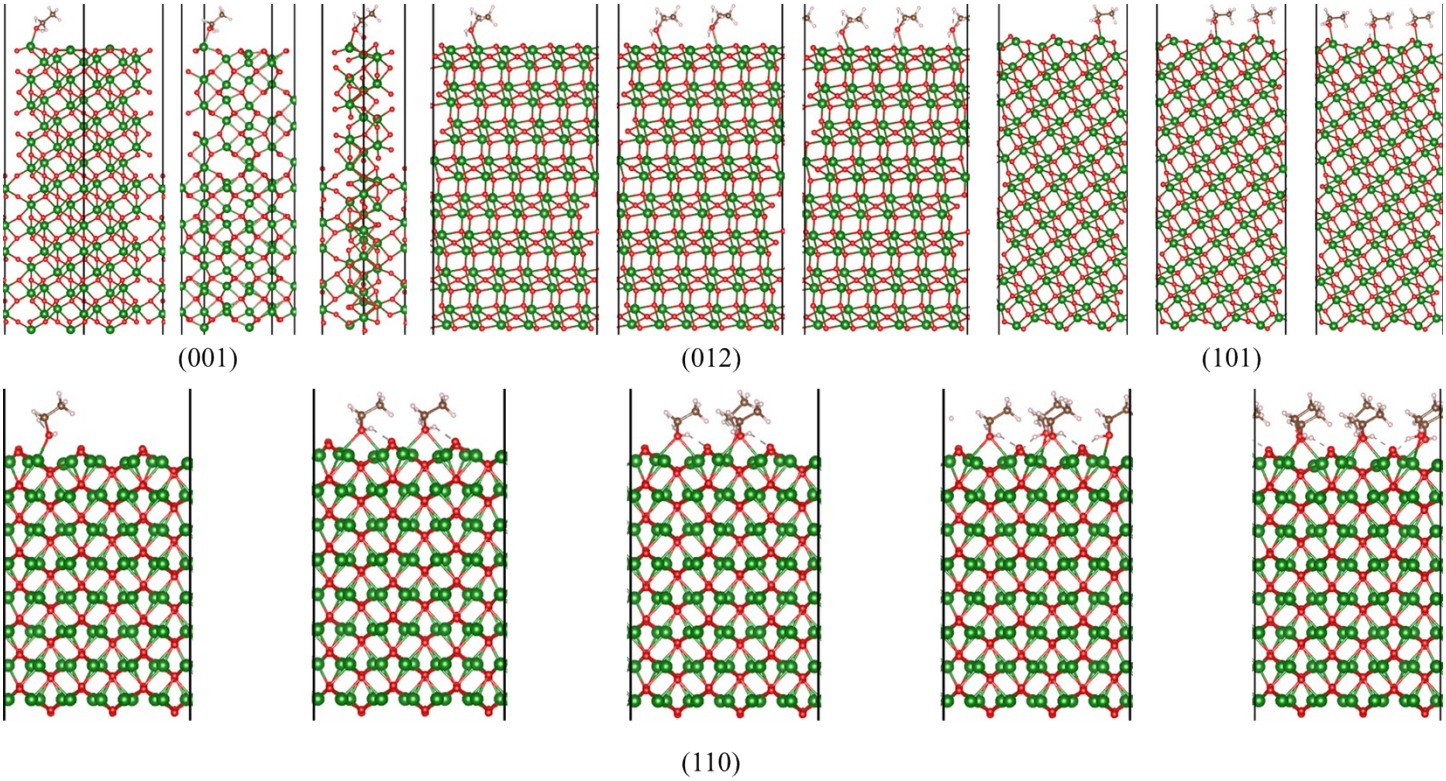

Figure S14. Optimised structure for ethanol chemisorbed on four surfaces at various coverage.

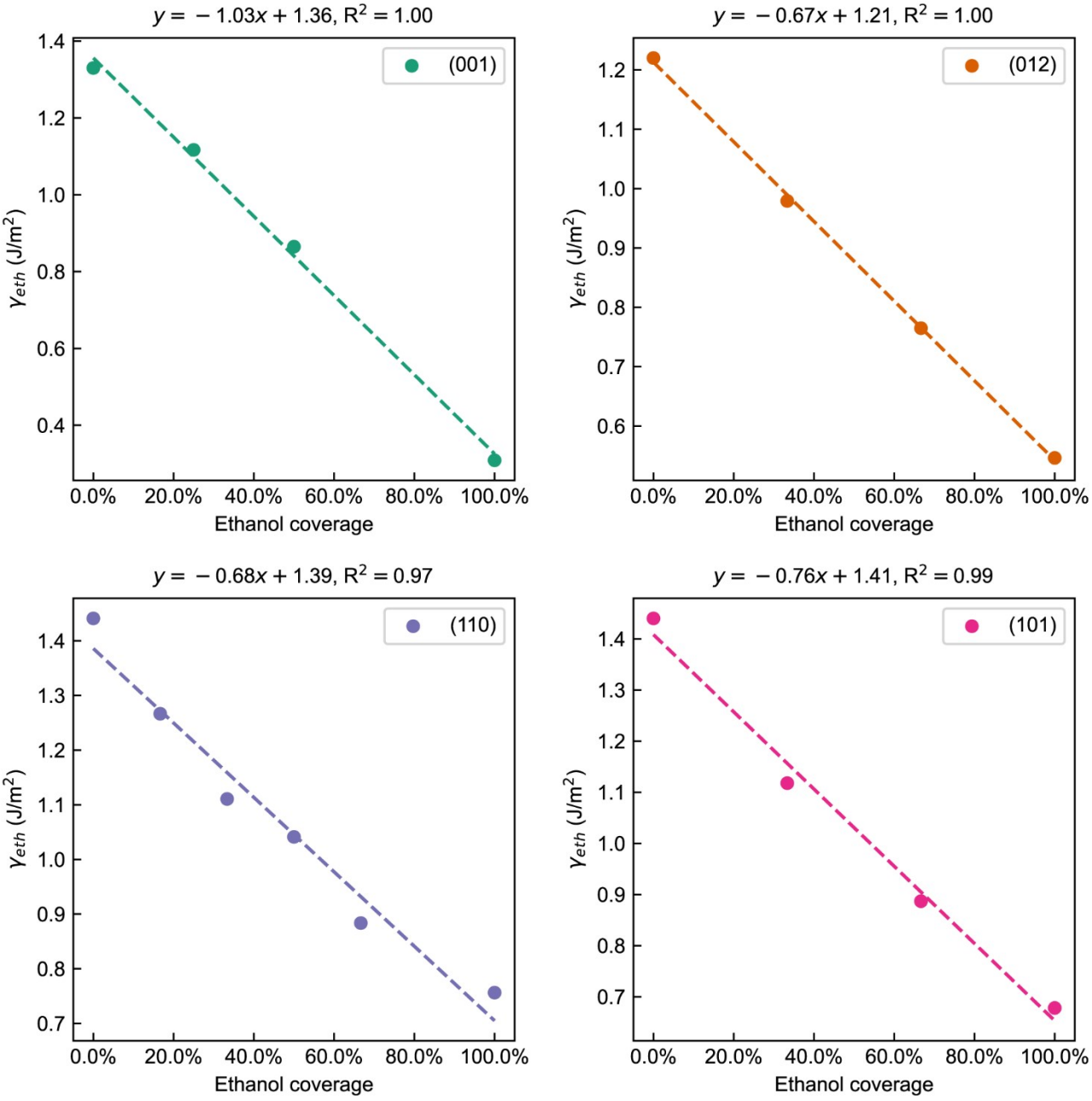

Figure S15. The linear relation between the specific surface energy and the ethanol coverage.

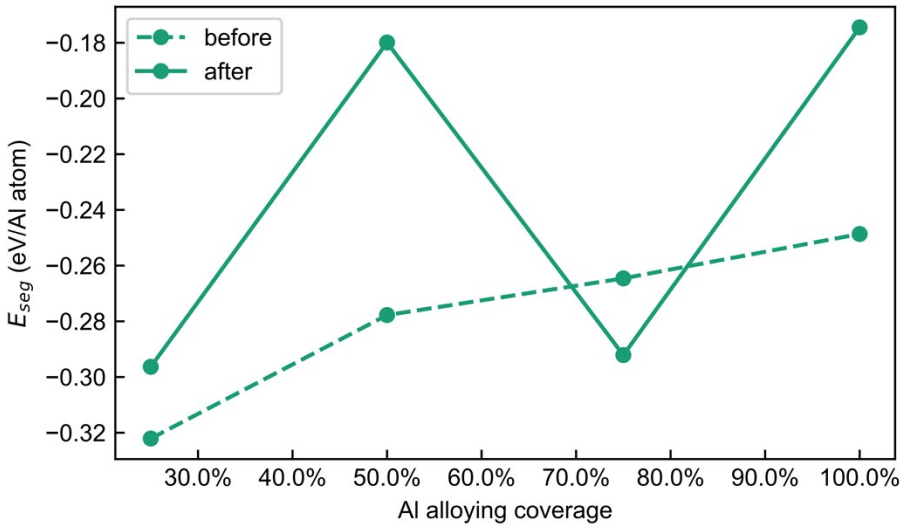

Figure S16. Al coverage-dependent E_{seg} under the complete capping of ethanol on the hematite (001) surface.

References

(1) Liu, J. Z.; van de Walle, A.; Ghosh, G.; Asta, M. Structure, Energetics, and Mechanical Stability of Fe-Cu Bcc Alloys from First-Principles Calculations. *Phys. Rev. B* **2005**, *72* (14), 144109.

(2) Lee, W. E.; Lagerlof, K. P. D. Structural and Electron Diffraction Data for Sapphire (α-Al_2O_3). *J. Electron Microsc. Tech.* **1985**, *2* (3), 247–258.

(3) Justus, J. S.; Roy, S. D. D.; Saravanakumar, K.; Raj, A. M. E. Judging Phase Purity of Hematite (α-Fe_2O_3) Nanoparticles through Structural and Magnetic Studies. *Mater. Res. Express* **2021**, *8* (5), 055005.

(4) Scholz, D.; Stirner, T. Convergence of Surface Energy Calculations for Various Methods: (001) Hematite as Benchmark. *J. Phys. Condens. Matter* **2019**, *31* (19), 195901.

(5) Mackrodt, W. C. Atomistic Simulation of Oxide Surfaces. *Phys. Chem. Miner.* **1988**, *15* (3), 228–237.

(6) Rohl, A. L.; Gay, D. H. Calculating the Effects of Surface Relaxation on Morphology. *J. Cryst. Growth* **1996**, *166* (1–4), 84–90.

(7) Guo, H.; Barnard, A. S. Thermodynamic Modelling of Nanomorphologies of Hematite and Goethite. *J. Mater. Chem.* **2011**, *21* (31), 11566–11577.

(8) Reeves, N. J.; Mann, S. Influence of Inorganic and Organic Additives on the Tailored Synthesis of Iron Oxides. *J. Chem. Soc. Faraday Trans.* **1991**, *87* (24), 3875–3880.